Supporting Information

Enhancing single-molecule magnet behaviour through decorating terminal ligands in Dy_2 compounds

Xiufang Ma,[a#] Bingbing Chen,[a#] Yi-Quan Zhang,[*b] Jinhui Yang,[a] Quan Shi,[*c] Yulong Ma,[a] and Xiangyu Liu*[a]

[a] *State Key Laboratory of High-efficiency Utilization of Coal and Green Chemical Engineering, National Demonstration Center for Experimental Chemistry Education, College of Chemistry and Chemical Engineering, Ningxia University, Yinchuan 750021, China*

[b] *Jiangsu Key Laboratory for NSLSCS, School of Physical Science and Technology, Nanjing Normal University, Nanjing 210023, China*

[c] *Dalian Institute of Chemical Physics, Chinese Academy of Sciences, 457 Zhongshan Road, Dalian 116023, China*

 # These authors contributed equally to this work.

***Corresponding author**

Dr. Xiangyu Liu

E-mail: xiangyuliu432@126.com

Dr. Yi-Quan Zhang

E-mail: zhangyiquan@njnu.edu.cn

Prof. Quan Shi

E-mail: shiquan@dicp.ac.cn

Contents

Scheme S1. Synthesis of the ligands H_2bfbpen and H_2bcbpen.

Figure S1. The ^{1}H NMR (a) and ^{13}C NMR (b) spectra of H_2bfbpen.

Figure S2. The ^{1}H NMR (a) and ^{13}C NMR (b) spectra of H_2bcbpen.

Figure S3. Molecular stacking charts of compounds **1** (a) and **2** (b). All hydrogen atoms and free iodide ions/H_2O are omitted for clarity.

Figure S4. PXRD curves of **1** (a) and **2** (b).

Figure S5. *M* vs *H* curves for **1** (a) and **2** (b) at different temperatures.

Figure S6. Temperature dependence of χ' and χ'' susceptibilities for **1** without static field.

Figure S7. Temperature dependence of χ' and χ'' susceptibilities for **2** without static field.

Figure S8. Temperature dependence of χ' and χ'' susceptibilities for **1** at applied DC fields of 1200 Oe.

Figure S9. Cole-Cole plots for **1** at applied DC fields of 1200 Oe. The solid lines represent the best fit to the measured results.

Figure S10. Hysteresis loops for **1** (a) and **2** (b) at 1.8 K.

Figure S11. C_p *vs* T plot for **1** (a) and **2** (b) at several magnetic fields.

Figure S12. Calculated model structures of individual Dy^{III} fragments of **1** and **2**. All hydrogen atoms and free iodide ions/H_2O are omitted for clarity.

Table S1. Crystal Data and Structure Refinement Details for **1** and **2**.

Table S2. Selected bond lengths (Å) and bond angles (°) for **1** and **2**.

Table S3. The calculated results for Dy^{III} ions configuration of **1** and **2** by SHAPE 2.1 software.

Table S4. Relaxation fitting parameters from least-squares fitting of $\chi(f)$ data under zero dc field of **1**

Table S5. Relaxation fitting parameters from least-squares fitting of $\chi(f)$ data under zero dc field of **2**

Table S6. Relaxation fitting parameters from least-squares fitting of $\chi(f)$ data under 1200 Oe dc field of **1**.

Table S7. Calculated energy levels (cm^{-1}), $\boldsymbol{g}$ (g_x, g_y, g_z) tensors and m_J values of the lowest eight Kramers doublets (KDs) of individual Dy^{III} fragments of **1** and **2** using CASSCF/RASSI with MOLCAS 8.2.

Table S8. Wave functions with definite projection of the total moment $| m_J >$ for the lowest two KDs of individual Dy^{III} fragments of **1** and **2** using CASSCF/RASSI with MOLCAS 8.2.

Table S9. Exchange energies (cm^{-1}), the corresponding tunneling gaps (Δ_{tun}) and the main values of the g_z for the lowest two exchange doublets of **1** and **2**.

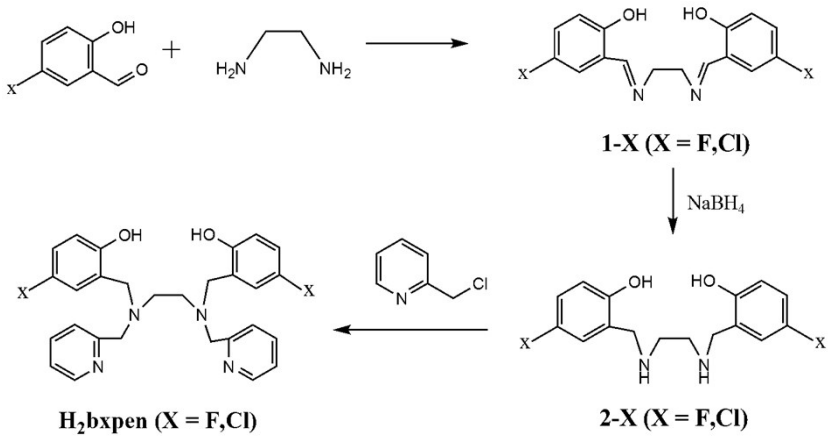

Scheme S1. Synthesis of the ligands H_2bfbpen and H_2bcbpen.

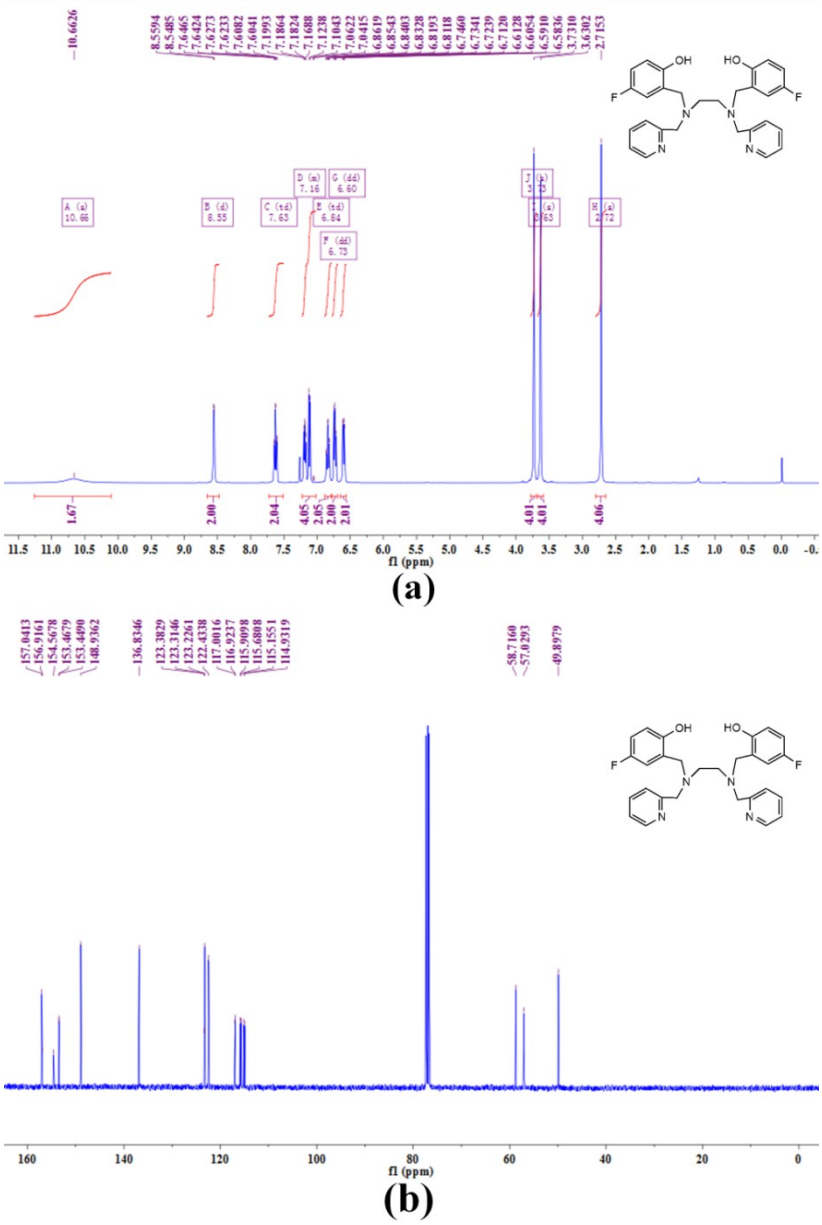

Figure S1. The ^{1}H NMR (a) and ^{13}C NMR (b) spectra of H_2bfbpen.

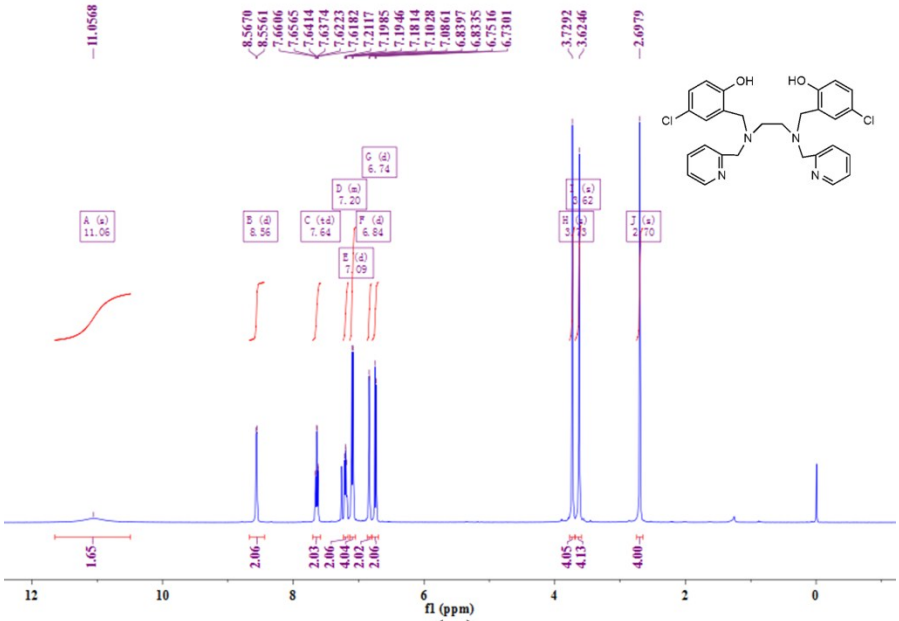

(a)

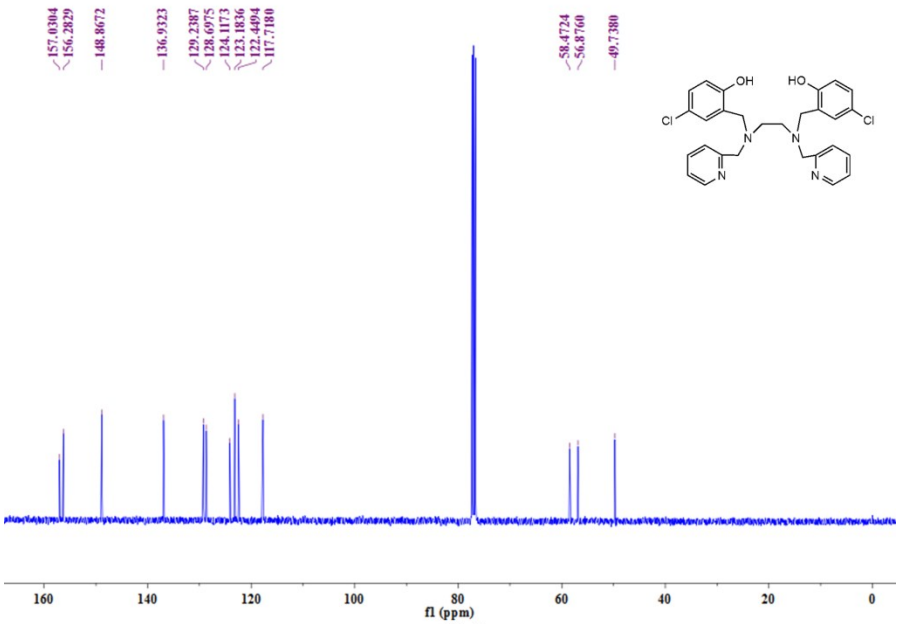

(b)

Figure S2. The ^{1}H NMR (a) and ^{13}C NMR (b) spectra of H_2bcbpen.

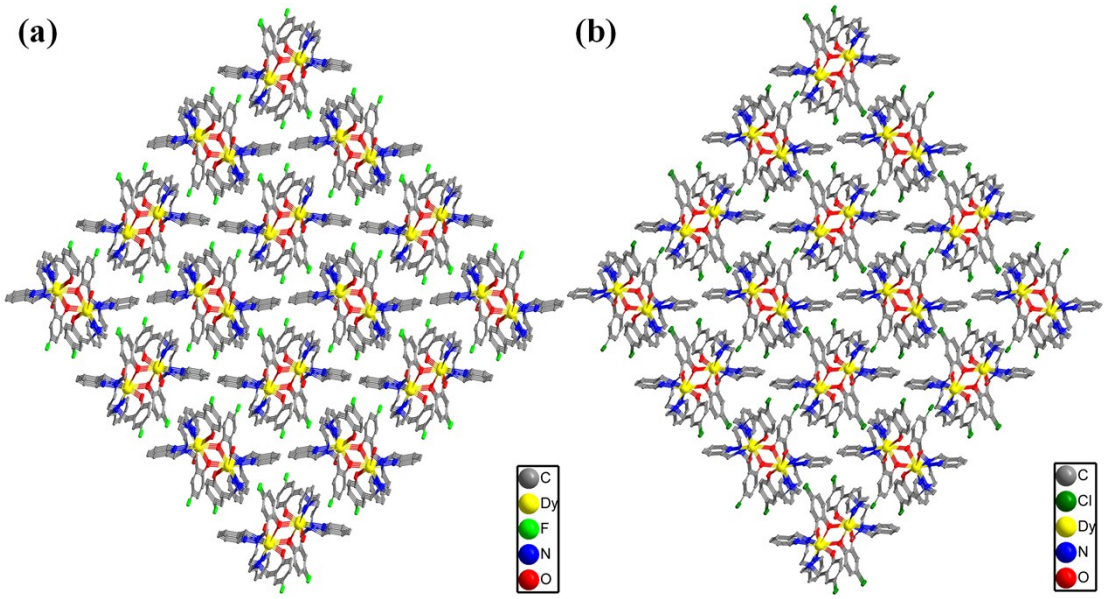

Figure S3. Molecular stacking charts of compounds **1** (a) and **2** (b). All hydrogen atoms and free iodide ions/H_2O are omitted for clarity.

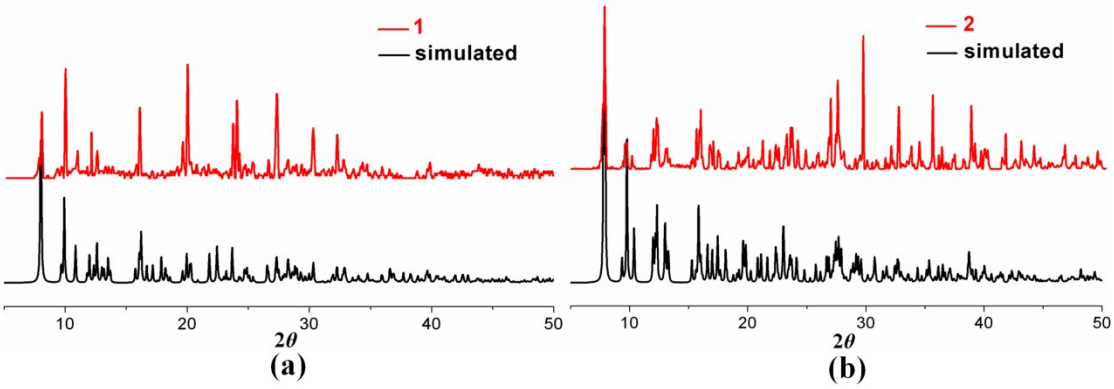

Figure S4. PXRD curves of **1** (a) and **2** (b).

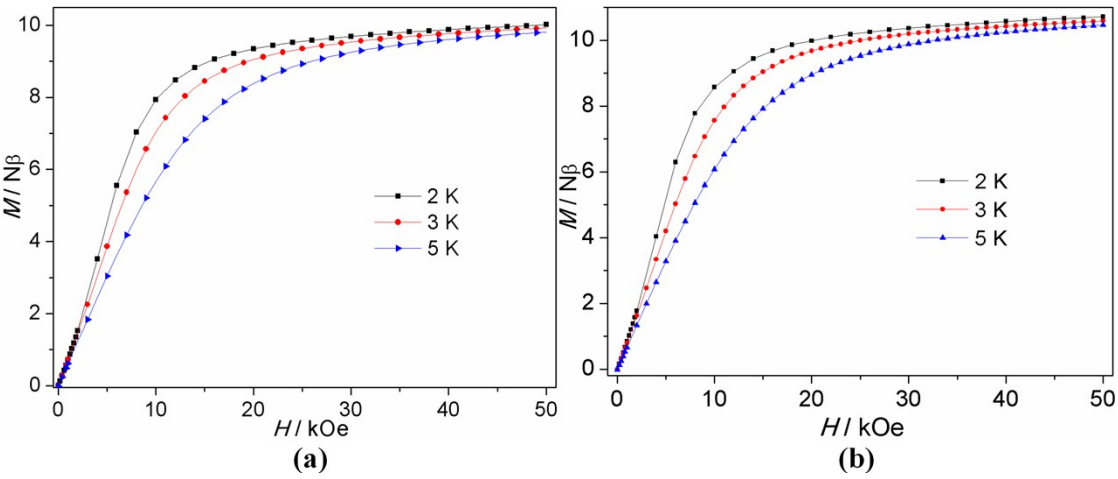

Figure S5. *M* vs *H* curves for **1** (a) and **2** (b) at different temperatures.

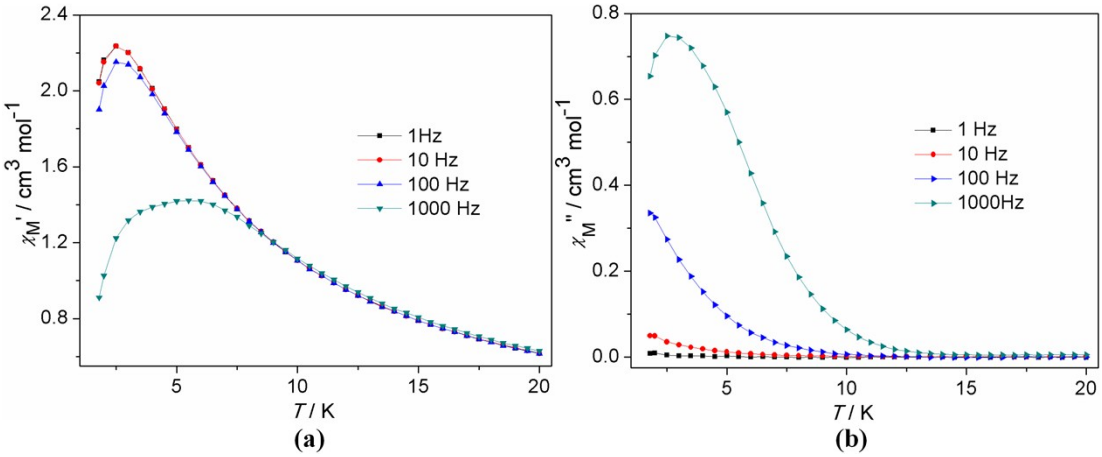

Figure S6. Temperature dependence of χ' and χ'' susceptibilities for **1** without static field.

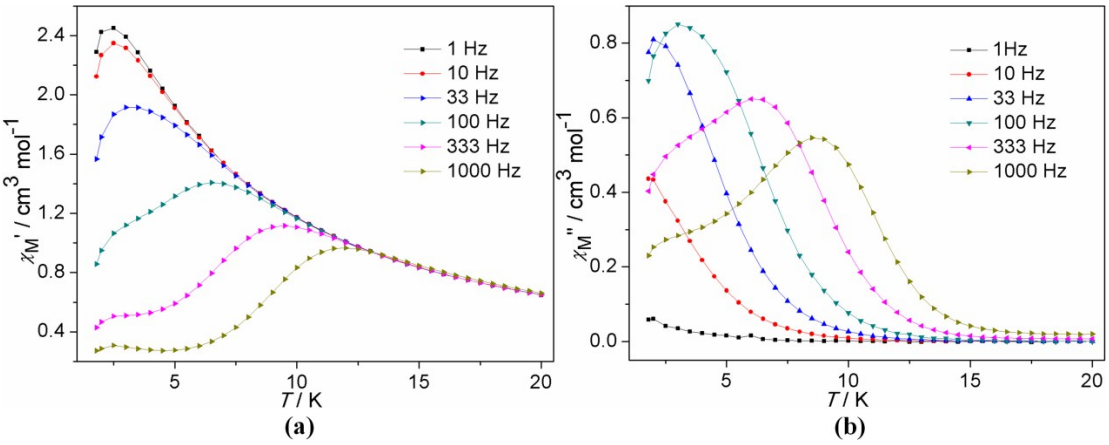

Figure S7. Temperature dependence of χ' and χ'' susceptibilities for **2** without static field.

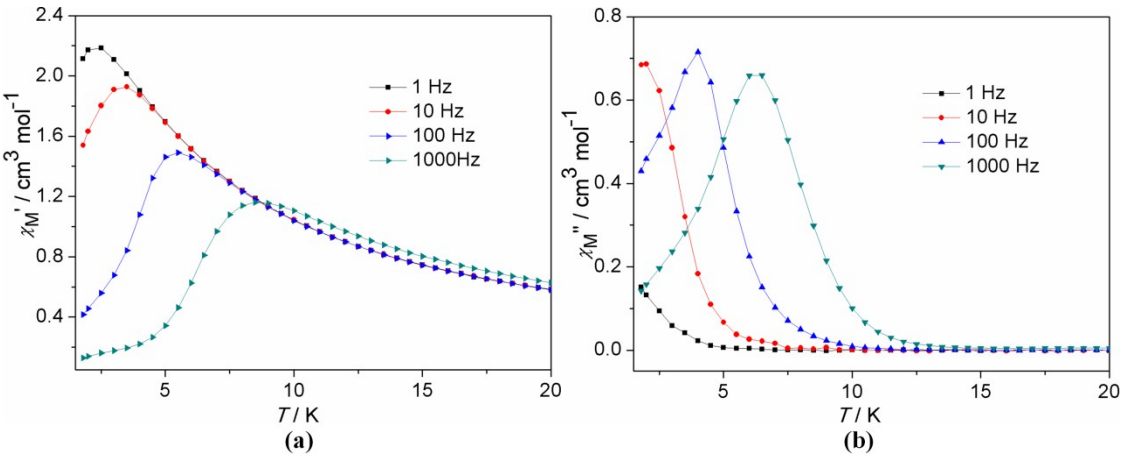

Figure S8. Temperature dependence of χ' and χ'' susceptibilities for **1** at applied dc fields of 1200 Oe.

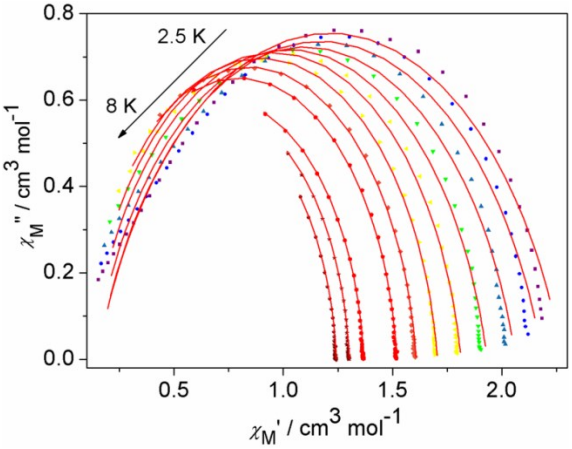

Figure S9. Cole-Cole plots for **1** at applied dc fields of 1200 Oe. The solid lines represent the best fit to the measured results.

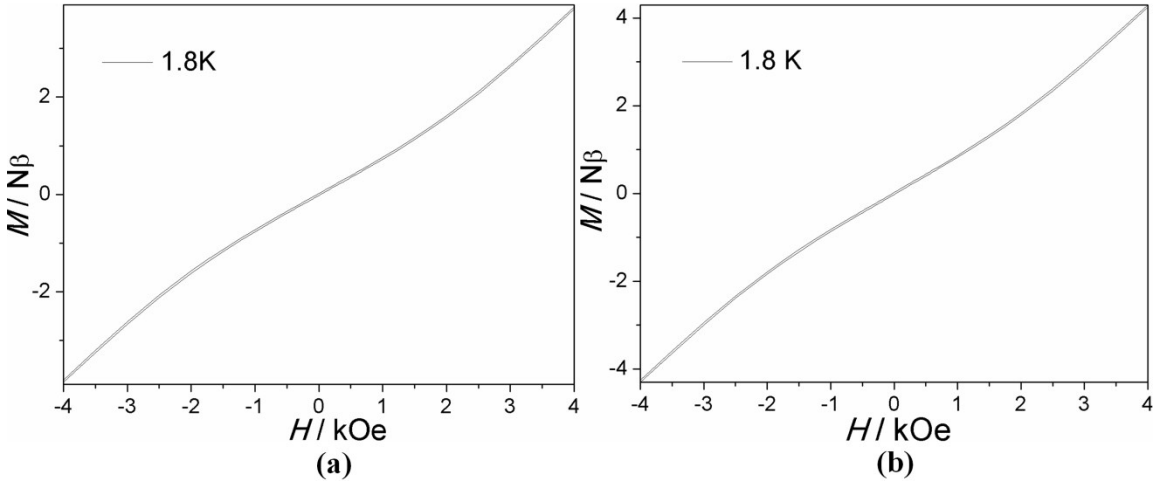

Figure S10. Hysteresis loops for **1** (a) and **2** (b) at 1.8 K.

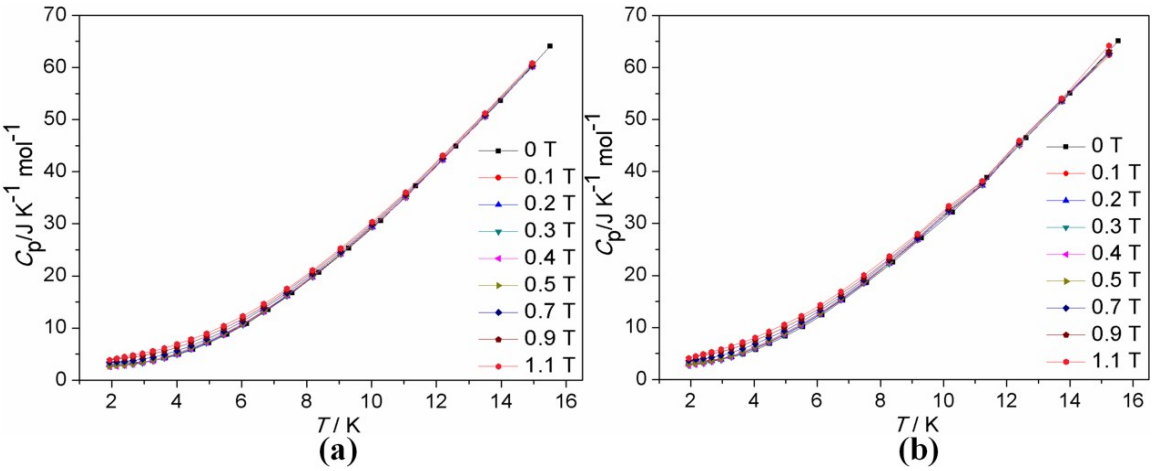

Figure S11. C_p *vs* T plot for **1** (a) and **2** (b) at several magnetic fields.

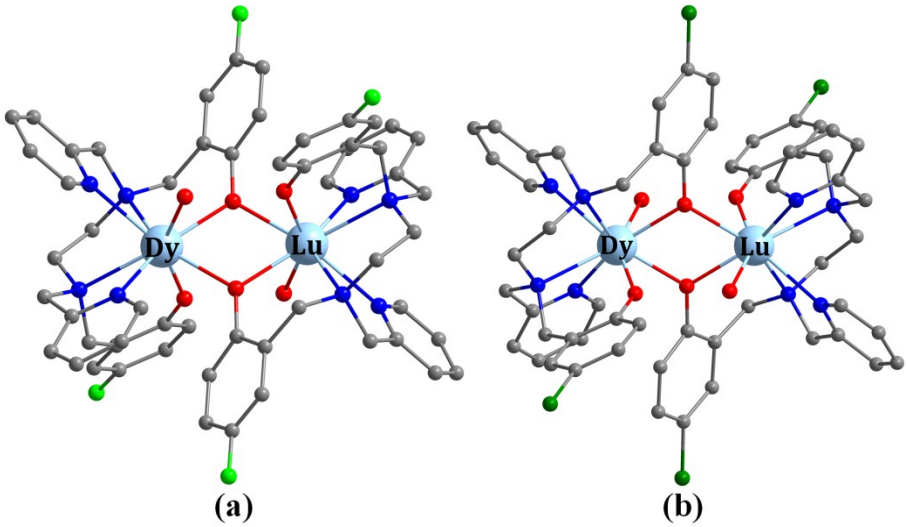

Figure S12. Calculated model structures of individual Dy^{III} fragments of **1** and **2**. All hydrogen atoms and free iodide ions/H_2O are omitted for clarity.

Table S1. Crystal Data and Structure Refinement Details for **1** and **2**.

	1	2
Empirical formula	$C_{56}H_{56}Dy_2F_4N_8O_6I_2$	$C_{56}H_{57}Dy_2Cl_4N_8O_{6.5}I_2$
Formula weight	1591.88	1666.42
Crystal system	monoclinic	monoclinic
Space group	$P2_1/c$	$P2_1/c$
a (Å)	11.6015(5)	11.8909(8)
b (Å)	16.2765(8)	17.0320(9)
c (Å)	15.7772(8)	15.4647(10)
α (°)	90	90
β (°)	108.453(2)	107.506(2)
γ (°)	90	90
V (Å^3)	2826.1(2)	2986.9(3)
Z	2	2
μ (mm^{-1})	3.786	3.751
Unique reflections	5161	5483
Observed reflections	3934	3679
R_{int}	0.050	0.079
Final R indices [$I > 2\sigma(I)$]	$R_1 = 0.0334$, $wR_2 = 0.0640$	$R_1 = 0.0495$, $wR_2 = 0.0846$
R indices (all data)	$R_1 = 0.0583$, $wR_2 = 0.0725$	$R_1 = 0.0968$, $wR_2 = 0.0998$

Table S2. Selected bond lengths (Å) and bond angles (°) for **1** and **2**.

1		2	
Dy(1)-O(1)	2.261(3)	Dy(1)-O(1)	2.248(5)
Dy(1)-O(2)	2.305(3)	Dy(1)-O(2)	2.311(5)
Dy(1)-O(3)	2.399(4)	Dy(1)-O(3)	2.382(7)
Dy(1)-N(1)	2.598(5)	Dy(1)-N(1)	2.614(7)

Dy(1)-N(2)	2.567(5)	Dy(1)-N(2)	2.547(7)
Dy(1)-N(3)	2.511(5)	Dy(1)-N(3)	2.522(7)
Dy(1)-N(4)	2.593(5)	Dy(1)-N(4)	2.601(6)
Dy(1)-O(2a)	2.405(3)	Dy(1)-O(2a)	2.402(5)
F(1)-C(10)	1.372(7)	Cl(1)-C(10)	1.752(9)
F(2)-C(23)	1.358(8)	Cl(2)-C(23)	1.722(11)
O(1)-Dy(1)-O(2)	84.42(12)	O(1)-Dy(1)-O(2)	83.75(18)
O(1)-Dy(1)-O(3)	149.44(13)	O(1)-Dy(1)-O(3)	149.75(19)
O(1)-Dy(1)-N(1)	74.10(13)	O(1)-Dy(1)-N(1)	73.39(19)
O(1)-Dy(1)-N(2)	81.09(14)	O(1)-Dy(1)-N(2)	80.29(19)
O(1)-Dy(1)-N(3)	110.03(14)	O(1)-Dy(1)-N(3)	110.7(2)
O(1)-Dy(1)-N(4)	139.76(14)	O(1)-Dy(1)-N(4)	139.1(2)
O(2)-Dy(1)-O(2a)	75.83(12)	O(2)-Dy(1)-O(2a)	76.90(17)
O(2)-Dy(1)-O(3)	73.83(13)	O(2)-Dy(1)-O(3)	74.1(2)
O(2)-Dy(1)-N(1)	146.67(14)	O(2)-Dy(1)-N(1)	146.2(2)
O(2)-Dy(1)-N(2)	80.16(14)	O(2)-Dy(1)-N(2)	80.04(19)
O(2)-Dy(1)-N(3)	146.67(14)	O(2)-Dy(1)-N(3)	147.3(2)
O(2)-Dy(1)-N(4)	109.65(13)	O(2)-Dy(1)-N(4)	110.68(19)
O(2)-Dy(1)-O(2a)	70.55(11)	O(2)-Dy(1)-O(2a)	69.99(17)
O(3)-Dy(1)-N(1)	134.39(15)	O(3)-Dy(1)-N(1)	135.0(2)
O(3)-Dy(1)-N(2)	115.00(15)	O(3)-Dy(1)-N(2)	114.9(2)
O(3)-Dy(1)-N(3)	80.05(15)	O(3)-Dy(1)-N(3)	80.4(2)
O(3)-Dy(1)-N(4)	69.39(15)	O(3)-Dy(1)-N(4)	69.7(2)
O(2a)-Dy(1)-O(3)	76.81(13)	O(2a)-Dy(1)-O(3)	76.30(19)
N(1)-Dy(1)-N(2)	71.68(15)	N(1)-Dy(1)-N(2)	71.9(2)
N(1)-Dy(1)-N(3)	66.25(15)	N(1)-Dy(1)-N(3)	66.0(2)
N(1)-Dy(1)-N(4)	74.61(15)	N(1)-Dy(1)-N(4)	74.7(2)
O(2a)-Dy(1)-N(1)	125.85(13)	O(2a)-Dy(1)-N(1)	125.98(18)
N(2)-Dy(1)-N(3)	130.55(15)	N(2)-Dy(1)-N(3)	130.1(2)
N(2)-Dy(1)-N(4)	65.42(15)	N(2)-Dy(1)-N(4)	65.8(2)

Table S3. The calculated results for Dy^{III} ions configuration of **1** and **2** by SHAPE 2.1 software.

Dy^{III} ion geometry analysis of **1**.

HBPY-8	3 D6h	Hexagonal bipyramid
CU-8	4 Oh	Cube
SAPR-8	5 D4d	Square antiprism
TDD-8	6 D2d	Triangular dodecahedron
JGBF-8	7 D2d	Johnson gyrobifastigium J26
JETBPY-8	8 D3h	Johnson elongated triangular bipyramid J14
JBTPR-8	9 C2v	Biaugmented trigonal prism J50
BTPR-8	10 C2v	Biaugmented trigonal prism
JSD-8	11 D2d	Snub diphenoid J84
TT-8	12 Td	Triakis tetrahedron
ETBPY-8	13 D3h	Elongated trigonal bipyramid

Structure [ML8]	HBPY-8	CU-8	SAPR-8	TDD-8	JGBF-8	JETBPY-8	JBTPR-8	BTPR-8	JSD-8	TT-8	ETBPY-8
ABOXIY ,	16.557,	10.661,	0.753,	1.900,	14.132,	27.250,	2.275,	2.069,	4.029,	11.292,	23.412

Dy^{III} ion geometry analysis of **2**.

HBPY-8 3 D6h Hexagonal bipyramid
CU-8 4 Oh Cube
SAPR-8 5 D4d Square antiprism
TDD-8 6 D2d Triangular dodecahedron
JGBF-8 7 D2d Johnson gyrobifastigium J26
JETBPY-8 8 D3h Johnson elongated triangular bipyramid J14
JBTPR-8 9 C2v Biaugmented trigonal prism J50
BTPR-8 10 C2v Biaugmented trigonal prism
JSD-8 11 D2d Snub diphenoid J84
TT-8 12 Td Triakis tetrahedron
ETBPY-8 13 D3h Elongated trigonal bipyramid

Structure [ML8]	HBPY-8	CU-8	SAPR-8	TDD-8	JGBF-8	JETBPY-8	JBTPR-8	BTPR-8	JSD-8	TT-8	ETBPY-8
ABOXIY ,	16.627,	10.837,	0.730,	2.058,	14.212,	27.257,	2.273,	2.111,	4.209,	11.493,	23.310

Configuration	ABOXIY, **1**	ABOXIY, **2**
Hexagonal bipyramid (D_{6h})	16.557	16.627
Cube (O_h)	10.661	10.837
Square antiprism (D_{4d})	**0.753**	**0.730**
Triangular dodecahedron (D_{2d})	1.900	2.058
Johnson gyrobifastigium J26 (D_{2d})	14.132	14.212
Johnson elongated triangular bipyramid J14 (D_{3h})	27.250	27.257
Biaugmented trigonal prism J50 (C_{2v})	2.275	2.273
Biaugmented trigonal prism (C_{2v})	2.069	2.111
Snub siphenoid J84 (D_{2d})	4.029	4.209
Triakis tetrahedron(T_d)	11.292	11.493
Elongated trigonal bipyramid(D_{3h})	23.412	23.310

Table S4. Relaxation fitting parameters from least-squares fitting of $\chi(f)$ data under zero dc field of **1**.

T(K)	χ_T	χ_S	α
2.4	2.244	0.371	0.139
2.8	2.230	0.389	0.129
3.2	2.175	0.391	0.119
3.4	2.139	0.393	0.113
3.8	2.057	0.378	0.103
4.2	1.970	0.363	0.092
4.4	1.926	0.347	0.087
5	1.799	0.302	0.072
5.5	1.700	0.236	0.063
6	1.609	0.132	0.059
7	1.448	0.000	0.039

Table S5. Relaxation fitting parameters from least-squares fitting of $\chi(f)$ data under zero dc field of **2**.

T(K)	χ_T	χ_S	α
2.5	2.489	0.241	0.155
3	2.425	0.224	0.143
3.5	2.312	0.207	0.133
4	2.186	0.191	0.124
4.5	2.059	0.178	0.114
5	1.938	0.166	0.104
5.5	1.827	0.154	0.096
6	1.724	0.142	0.090
6.5	1.632	0.134	0.082
7	1.546	0.127	0.075
7.5	1.469	0.122	0.067
8	1.399	0.118	0.060
8.5	1.335	0.116	0.044
9	1.276	0.111	0.038
9.5	1.222	0.105	0.032
10	1.171	0.092	0.029
11	1.083	0.000	0.003
12	1.007	0.000	0.052

Table S6. Relaxation fitting parameters from least-squares fitting of $\chi(f)$ data under 1200 Oe dc field of **1**.

T(K)	χ_T	χ_S	α
2.4	2.277	0.144	0.215
2.8	2.186	0.145	0.204
3.2	2.061	0.131	0.181
3.4	1.930	0.112	0.149
3.8	1.811	0.096	0.119
4.2	1.703	0.086	0.093
4.4	1.605	0.078	0.076
5	1.517	0.072	0.065
5.5	1.365	0.052	0.055
6	1.299	0.020	0.052
7	1.240	0.000	0.047

Table S7. Calculated energy levels (cm^{-1}), $\boldsymbol{g}$ (g_x, g_y, g_z) tensors and m_J values of the lowest eight Kramers doublets (KDs) of individual Dy^{III} fragments of **1** and **2** using CASSCF/RASSI with MOLCAS 8.2.

	1			**2**		
KDs	E/cm^{-1}	$\boldsymbol{g}$	m_J	E/cm^{-1}	$\boldsymbol{g}$	m_J
1	0.0	0.268 0.599 19.085	±15/2	0.0	0.093 0.178 19.525	±15/2

2	66.9	1.439 2.016 16.380	±1/2	103.7	1.958 4.165 14.906	±5/2
3	124.7	0.155 2.929 12.921	±13/2	144.0	1.359 3.800 11.932	±13/2
4	168.2	1.199 2.723 14.329	±3/2	207.0	1.569 2.382 10.232	±3/2
5	201.4	7.667 6.159 1.257	±7/2	232.9	0.943 3.434 9.100	±9/2
6	233.9	2.299 6.215 10.973	±9/2	257.5	8.731 6.391 3.919	±7/2
7	303.0	0.503 0.719 18.134	±5/2	323.1	0.751 1.146 17.632	±1/2
8	520.9	0.001 0.006 19.715	±11/2	561.3	0.005 0.011 19.725	±11/2

Table S8. Wave functions with definite projection of the total moment | m_J > for the lowest two KDs of individual Dy^{III} fragments of **1** and **2** using CASSCF/RASSI with MOLCAS 8.2.

	E/cm^{-1}	wave functions
1	0.0	43%|+15/2>
	0.0	49%|-15/2>
	66.9	10%|±13/2>+14%|±5/2>+24%|±3/2>+38%|±1/2>
2	0.0	90%|+15/2>
	0.0	7%|-15/2>
	103.7	20%|±13/2>+17%|±5/2>+21%|±3/2>+25%|±1/2>

Table S9. Exchange energies (cm^{-1}), the corresponding tunneling gaps (Δ_{tun}) and the main values of the g_z for the lowest two exchange doublets of **1** and **2**.

	1			**2**		
	E/cm^{-1}	Δ_t	g_z	E/cm^{-1}	Δ_t	g_z
1	0.0	1.5×10^{-3}	0.000	0.0	1.0×10^{-4}	0.000
2	1.7	2.5×10^{-3}	38.150	1.8	2.3×10^{-4}	39.045